White Paper: 52608

Principles and Applications of Parallel Beam Wavelength Dispersive X-ray Spectroscopy

Key Words

Accelerating Voltage; Bragg's Law, EDS, Energy Dispersive X-ray Spectroscopy, Freibergite, Geochronology, Nanoanalysis, Parallel Beam WDS, Rowland Circle, Wavelength Dispersive X-ray Spectroscopy, WDS

Introduction

Chemical analysis using the scanning electron microscope (SEM) is accomplished using either Energy Dispersive X-ray Spectroscopy (EDS) or Wavelength Dispersive X-ray Spectroscopy (WDS). Both techniques analyze the characteristic X-rays emitted from a sample upon the exposure of a sample to an electron beam. With EDS, a very wide range (i.e., nearly all) of X-ray energy lines are collected simultaneously. With WDS, a single X-ray energy – monochromatic X-rays – are counted at any given time.

The first WDS spectrometers were constructed with a Rowland circle technique (e.g., Castaing, 1951[1]; JEOL L-Value table[2]; CAMECA® SXFiveFE brochure[3]; Oxford Instruments Wave brochure[4]; Thermo Scientific™ NORAN™ IbeX[5]). The next generation of WDS spectrometers involved the use of a parallel beam wavelength-dispersive spectrometer, which improved the X-ray collection efficiency in the low energy (i.e., <1.5k eV) range of the spectrum at the expense of X-ray collection efficiency in the moderate to higher energy ranges (i.e., >2.5 keV; see the EDAX LEXS product bulletin[6] and the Bruker XSense flyer[7]). The most recent generation of WDS spectrometers utilized a parallel beam spectrometer with a hybrid X-ray optic that enabled high X-ray collection efficiency in both the low and high energy parts of the spectrum.

This paper reviews the fundamental principles of WDS and explores the technical evolution of the technique.

Principles of WDS

WDS is based on Bragg's Law of diffraction:

$$n\lambda = 2d \sin\theta \qquad \text{Equation 1}$$

where λ (nm) is the X-ray wavelength of interest, d (nm) is the interplanar spacing of the diffractor, θ is the angle of X-ray incidence on the diffractor, n is an integer and

$$E(\text{keV}) = \frac{1.2398}{n\lambda} \qquad \text{Equation 2a}$$

or

$$E(\text{keV}) = \frac{1.2398n}{2d\sin\theta} \qquad \text{Equation 2b}$$

The theoretical basis of WDS, therefore, is quite straight-forward. The material under study generates characteristic X-rays. These X-rays are diffracted by a diffractor with a well-defined 2d spacing, and the diffracted X-rays are counted using a detector. The geometry of the WD spectrometer is systematically adjusted to select the specific X-ray energy line(s) of interest.

Thermo SCIENTIFIC

The geometry of the WD spectrometer is primarily adjusted by changing the angle, θ, of the diffractor relative to the sample. This angle determines the X-ray energy that satisfies Bragg's Law. That characteristic X-ray energy corresponds to a specific element(s). By adjusting the angle of the diffractor relative to the sample, a range of X-ray energies can be analyzed using WDS. The relative intensity of X-rays measured at each specific geometry indicates the relative abundance of the elements present in the sample under study. In this way, WDS is routinely used to quantify elemental concentrations with an accuracy of ~0.1%.

It is worth noting that Bragg's Law allows for higher order reflections (n = 2, 3, 4…) in the WD spectrum. For example, the Ag $L\alpha_1$ X-ray has an energy of 2.984 keV. Using a PET crystal as the diffractor, this corresponds to an angle, θ, of 28.38°. If the WD spectrometer is tuned to count X-rays at 1.492 keV (θ = 71.91° on the same crystal), and if the same Ag sample was analyzed, the WD spectrometer may measure a smaller amount of 2nd order (i.e. n = 2) Ag $L\alpha_1$ X-rays (Figure 1).

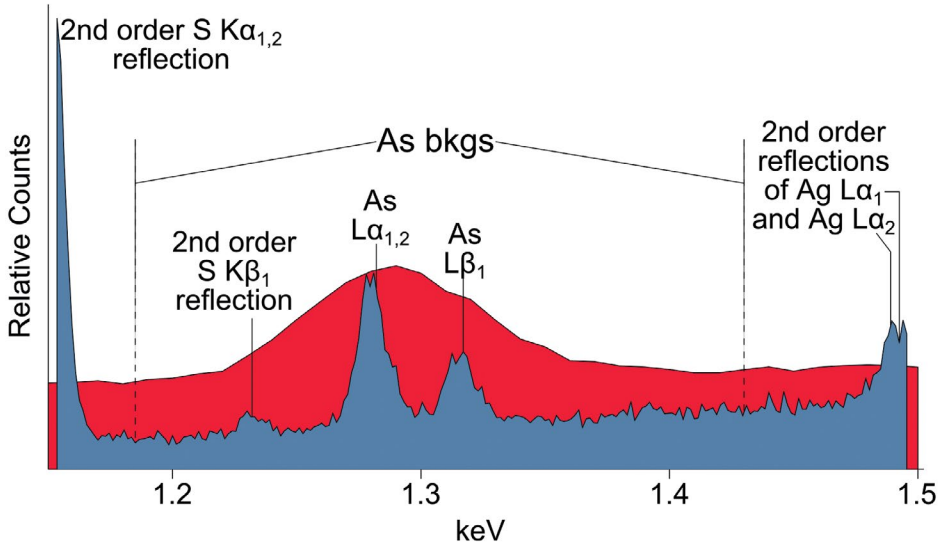

Figure 1: ED spectrum (red) and WDS energy scan (blue) of the As L-line spectral region of freibergite ($[Cu,Zn,Ag]_{12}[Sb,As]_4S_{13}$). 2nd order reflections of S $K_{1,2}$ (1.154 keV), S $K\beta_1$ (1.232 keV), and Ag $L\alpha_{1,2}$ (1.491 keV) are present in this spectral region. In order to correctly quantify the As concentration or As $L\alpha_{1,2}$ peak-to-background, these 2nd order reflections must be avoided when selecting off-peak measurement positions.

This example demonstrates an important fact of WD spectroscopy. Although WDS results are typically reported as a function of either energy or wavelength, the physical spectrometer is actually testing for characteristic X-rays as a function of the angle between the diffractor and the sample. This leads to a series of very real geometric constraints regarding the practical and economical construction of a WDS spectrometer.

The classic derivation of Bragg's Law is as follows. Consider a parallel beam of X-rays of wavelength λ that is incident on a material, the structure of which comprises a precisely parallel arrangement of planes (atomic, molecular, or otherwise), with an interplanar spacing, d (Figure 2).

X-ray 1 is reflected into 1' from the top plane in the diffractor (or "crystal") with the angle of incidence, θ, equal to the angle of reflection. X-ray 2-2', being reflected from the lower plane, travels an extra distance in the material equal to d•sin θ + d•sin θ. For an intense diffracted beam to result at the detector, wave segments 1' and 2' must be in phase; which, in turn, requires that the extra path length travelled by wave 2-2' must be an integral number of wavelengths: that is, 2 (d•sin θ) must equal nλ. Bragg's Law is satisfied for various wavelengths emitted from the sample, with constructive interference resulting in a high intensity beam. The diffractor is highly reflective only at very specific Bragg angles, which is the key to the high spectral resolution of WDS.

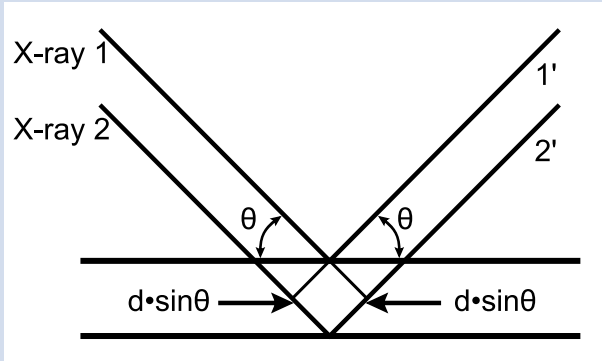

Figure 2: Schematic diagram showing the ray path of parallel X-rays between two diffracting planes.

Conventional WDS and Rowland Circle Approach

Conventional WDS systems consist of three main components: an X-ray source, a diffractor, and an X-ray detector. The X-ray source is the electron probe interaction volume on (or just below) the surface of the sample. The diffractor is a crystal or layered material with a known 2d spacing that diffracts only X-rays that satisfy Bragg's Law toward the detector. The X-ray detectors of most WDS spectrometers consist of a proportional counter which generates an electronic signal proportional to the numbers of X-rays interacting with a gas. Because the detector contains a gas, a window must be used to isolate the inside of the detector from the vacuum of the microscope and spectrometer. If low energy X-rays are to be analyzed, the window must be thin. In WDS systems, two types of detector are used. Gas-flow counters typically contain a P-10 gas (a mixture of 90% Ar and 10% CH_4). Sealed proportional counters contain Xe or Xe + CO_2.

Rowland circle WDS requires that the sample (i.e., the X-ray source), the diffractor, and the detector are situated on a Rowland circle of radius, R (Figure 3), in order to satisfy Bragg's Law. In this geometry, the distances from the source to the crystal and from the crystal to the detector are identical (hereafter, "L"). In the derivation of Bragg's Law, a parallel beam of X-rays is assumed. However, as a practical matter, X-rays emitted by a sample in an SEM or microprobe originate from a small interaction volume at (and just below) the sample surface and diverge from the origin as a hemispherical wave front (i.e., equally in all directions). Because flat diffractors do not focus or converge the diverging X-rays, a flat diffractor yields a very low count rate at the detector because the X-ray intensity falls quadratically as a function of the distance between the sample and the actual X-ray counter. As a result, a Rowland circle design with flat diffractor is inherently impractical (Figure 4).

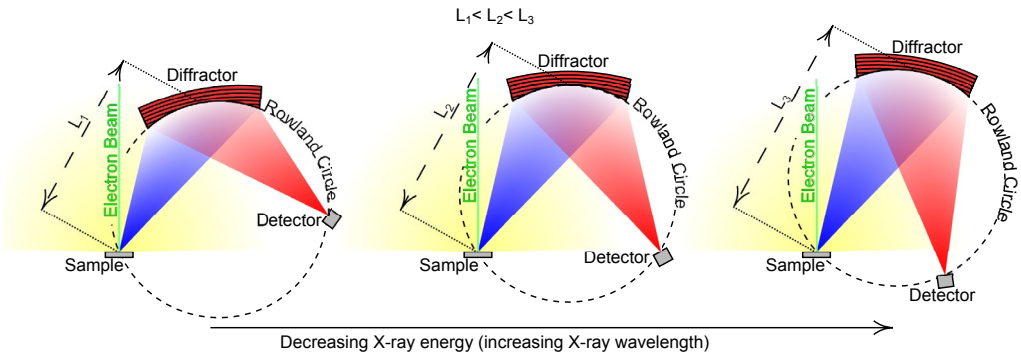

Figure 3: Diagrams of conventional WDS based on the Rowland circle using a Johansson diffractor (diffractor size is greatly exaggerated). The yellow area represents all X-rays emitted from the sample by the interaction of the electron beam with the sample. The blue area represents the subset of X-rays that will collide with the diffractor. The red area represents the X-rays that are reflected by the diffractor and are focused on the detector. From left to right, the spectrometer orientation changes to detect X-rays of lower energy. This change in orientation results in an increasing distance (L) between the sample (the X-ray source) and the diffractor. By increasing L, the X-ray intensity at the diffractor decreases because the X-ray intensity is proportional to $\frac{1}{L^2}$. The result of the Rowland circle orientation is that the collection of low energy X-rays (e.g., O Kα) is less efficient relative to high energy X-rays (e.g., Fe Kα).

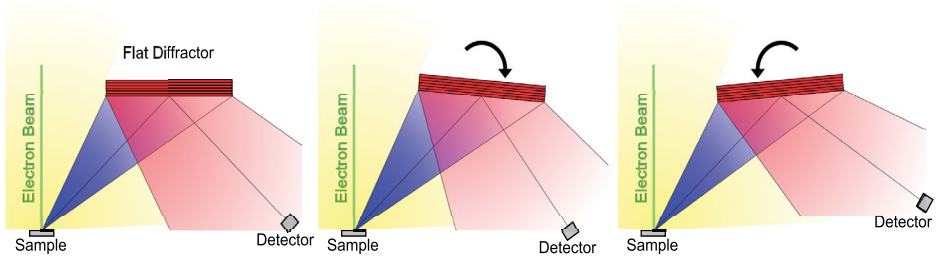

Figure 4: The yellow area represents all X-rays emitted from the sample by the interaction of the electron beam with the sample. The blue area represents the subset of X-rays that will collide with the diffractor. The red area represents the X-rays that are reflected by the diffractor. When diverging X-rays contact a flat diffractor, they reflect but continue to diverge yielding a low count rate at the detector.

Alternatively, curved diffractors are used in Rowland circle WDS systems to focus or converge the diverging X-rays onto the detector. A Johann diffractor consists of layers curved to radius, 2R (Figure 5, left). Johann diffractors do not truly focus the X-rays onto the detector but do converge the X-rays enough for practical use. True focusing is accomplished using a Johansson diffractor, which also consists of layers curved to radius, 2R, and is then ground to radius, R – the same curvature as the Rowland circle on which the diffractor is positioned (Figure 5, right). However, layered diffractors, typically used for the analysis of light elements, are particularly difficult (prohibitively so) to manufacture with the Johansson geometry. As a result, typical Rowland circle WD spectrometers include layered diffractors with Johann geometry and crystalline diffractors (e.g., TAP, PET, and LiF) with Johansson geometry.

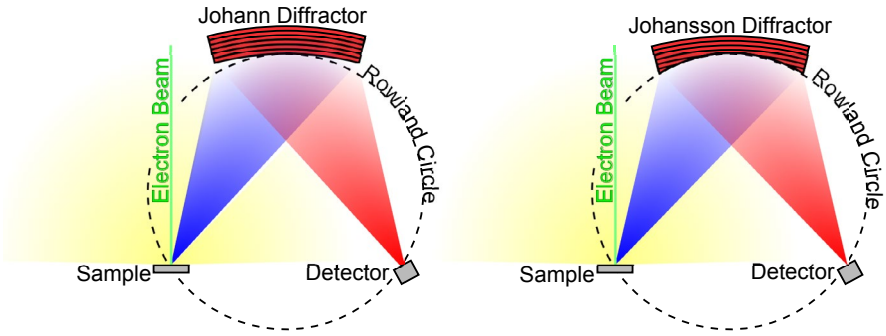

Figure 5: Diagrams of the two diffractor geometries, Johann and Johansson, used in Rowland circle WDS. The yellow area represents all X-rays emitted from the sample by the interaction of the electron beam with the sample. The blue area represents the subset of X-rays that will collide with the diffractor. The red area represents the X-rays that are reflected by the diffractor.

In order to position a Rowland circle spectrometer (Figure 6a) to count an X-ray of a certain wavelength, or to scan the spectrometer over a range of the energy spectrum, the angle, θ, with which the incident X-rays intersect the diffractor must change to satisfy Bragg's Law. The sample position must remain fixed. Therefore, the diffractor must rotate, changing the location of the focused (or converged) X-rays (Figure 6b). Because the detector cannot both remain on the Rowland circle and be at the point where the diffracted X-rays are focused (Figure 6c), the diffractor must move away from (or toward) the sample (i.e., the L distance must change) so that the following equation is true:

$$L = 2R \sin\theta = \frac{R\lambda}{d} \qquad \text{Equation 3}$$

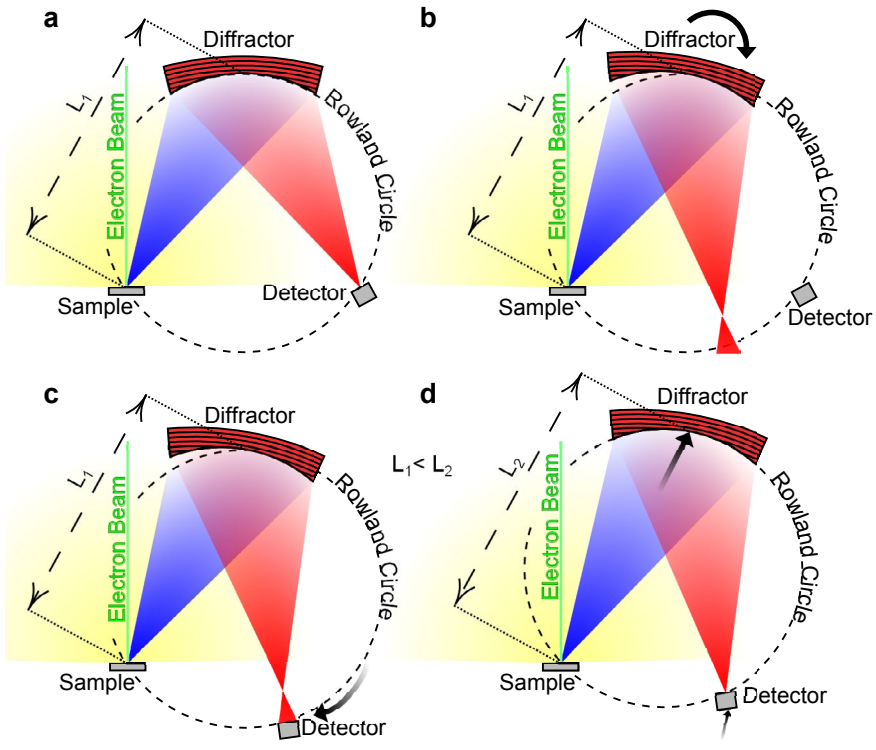

Figure 6: Diagrams of the movement required by the components of a Rowland circle WDS spectrometer for the detection of lower energy X-rays (i.e., the X-rays measured in d are of lower energy than would be measured in a). The yellow area represents all X-rays emitted from the sample by the interaction of the electron beam with the sample. The blue area represents the subset of X-rays that will collide with the diffractor (diffractor size is greatly exaggerated). The red area represents the X-rays that are reflected by the diffractor. From a to b, the diffractor rotates, changing the angle, θ, at which X-rays intersect the diffractor. The X-rays reflected off the diffractor (red) are focused at a different location. From b to c, the detector moves along the Rowland circle; however, the X-rays are not focused on the Rowland circle and are therefore not focused on the detector. From c to d, the diffractor moves away from the sample, and the detector must change position to stay on the Rowland circle focusing the diffracted X-rays on the detector.

Furthermore, the detector must move to the focus point of the diffracted X-rays (Figure 6d). In practice, Rowland circle spectrometers accomplish the motion of the diffractor and the detector by driving both to the necessary positions simultaneously, reducing the distance that the detector must be moved.

An important result of the aforementioned movement of the diffractor and detector associated with the positioning of a Rowland circle spectrometer is that **the distance between the sample and the diffractor changes with X-ray energy**. For a given diffractor, higher energy X-rays (i.e., shorter wavelengths) require Rowland circle geometries with a shorter L distances. Lower energy X-rays (i.e., longer wavelengths) require longer L distances (Figure 3). This presents practical geometry considerations because a Rowland circle WDS spectrometer will have physical limitations to the overall size and weight. It also presents a collection efficiency challenge at low energies.

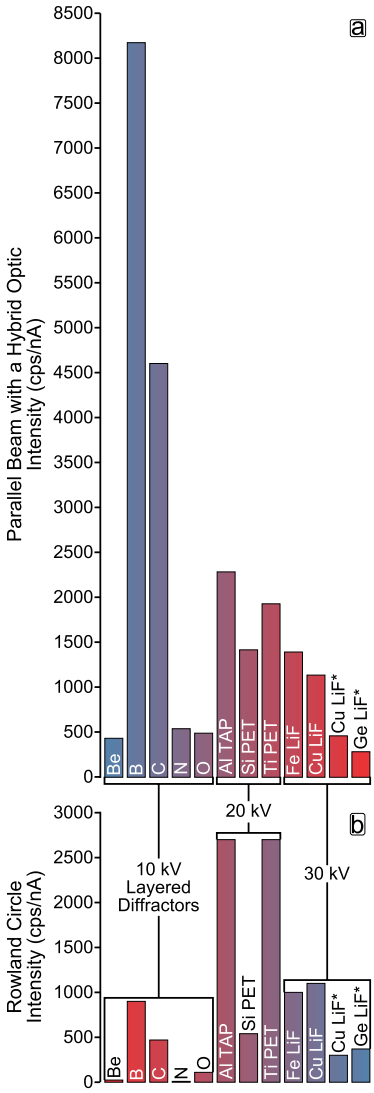

Figure 7: Expected intensities from a hybrid optic parallel beam WDS spectrometer (a) and a Rowland circle WDS spectrometer (b). Be, B, C, N, and O intensities were measured using layered diffractors with a 10 kV accelerating voltage. Al intensities were measured using a TAP crystal with a 20 kV accelerating voltage. Using a PET crystal, Si and Ti intensities were measured with a 20 kV accelerating voltage. Ti, Fe, Cu, and Ge were measured using LiF crystals with a 30 kV accelerating voltage. "LiF" refers to a LiF 200 crystal, and "LiF*" refers to a LiF 220 crystal. The difference between the two LiF crystals is that the LiF 220 has a smaller 2d spacing allowing it to be used for the analysis of higher energy X-rays compared to the more common LiF 200.

As the geometric L distance increases, the solid angle, Ω, decreases in quadratic fashion. The solid angle can be expressed either as a function of θ,

$$\Omega = \frac{A\sin\theta}{L^2} = \frac{A\sin\theta}{(2R\sin\theta)^2} = \frac{A}{4R^2\sin\theta} \qquad \text{Equation 4}$$

or as a function of wavelength, λ,

$$\Omega = \frac{A\frac{\lambda}{2d}}{L^2} = \frac{A\frac{\lambda}{2d}}{(\frac{R\lambda}{2d})^2} = \frac{Ad}{2R^2\lambda} \qquad \text{Equation 5}$$

in which "A" is the area of the diffractor, "d" is the interplanar spacing of the diffractor, and "R" is the radius of the Rowland circle. The numerators of Equations 4 and 5 contain a $\sin\theta$ or $\frac{\lambda}{(2d)}$ that account for the rotation of the diffractor, which mitigates the effect that increasing "L" has on the diffractor solid angle. However, the solid angle still decreases as "L" increases. For example, both Si Kα_1 and F Si Kα can be counted on a TAP crystal diffractor. Si Kα_1 has a wavelength of 0.7125 nm (1.740 keV), and F Kα has a wavelength of 1.8320 nm (0.677 keV). The wavelength of F Kα is ~2.5× that of Si Kα_1. Based on Equation 5, the solid angle of the TAP crystal when counting Si Kα_1 is ~2.5× the solid angle of the TAP crystal when counting F Kα. Therefore, the Si Kα_1 intensity counted on the TAP crystal is expected to be ~2.5× greater than the intensity counted for F Kα. The intensities that would be expected from using a Rowland circle WD spectrometer are plotted in the bottom of Figure 7.

Given Equations 4 and 5, there are two factors that could be addressed to improve the intensities counted on a Rowland circle spectrometer. A larger diffractor (bigger "A" in Equations 4 and 5) could be used. Larger diffractors are more expensive than small diffractors. Moreover, there is a practical limit to the size of a diffractor that can fit and operate within a spectrometer. A greater effect on intensity would result from choosing a spectrometer with a Rowland circle of smaller radius "R." If all other conditions are constant, a Rowland circle with a radius 50% that of another Rowland circle will yield 400% greater diffractor solid angle and therefore a greater intensity. However, a smaller Rowland circle constrains the diffractor size, reducing the solid angle gains of the smaller geometry. It also demands diffractor and detector drive motors capable of finer movements, resulting in a more expensive and less stable spectrometer.

Rowland circle WDS strongly relies on the sample (the X-ray source) being at the proper working distance. If the working distance is incorrect, then the sample does not lie on the Rowland circle, and the distance between the sample and the diffractor is not equal to the distance between the diffractor and the detector. Some electron microscopes (typically, electron microprobes) include optical microscopes. The optical image is in focus only when the sample is at the correct working distance and Z position. However, being that most SEMs are not equipped with an optical microscope, special care must be taken to ensure that the sample is at the proper working distance.

Rowland circle WDS strongly relies on the sample being at the proper working distance. If the working distance is incorrect, the sample does not lie on the Rowland circle and the distance between the sample and the diffractor is not equal to the distance between the diffractor and the detector.

Parallel Beam WDS

The motivation for the Rowland circle technique is to compensate for the divergent nature of X-ray emission from the sample surface. In parallel beam WDS systems, an X-ray optic placed near the sample in order to transform the divergent X-rays from the sample into a parallel beam. Therefore, a Rowland circle geometry is not required. This dramatically reduces the complexity of the spectrometer design and integration with the SEM. It also results in a relatively more compact spectrometer. The advantage of this approach is that the diffractor can be flat and placed at a semi-infinite distance from the sample without losing X-ray intensity (Figures 8 and 9). As a result, parallel beam WDS provides dramatically better sensitivity than traditional WDS, particularly at low energies (Figure 7). There are two X-ray optical technologies available for collimating diverging X-rays – grazing incidence and polycapillary optics. For low energies (< ~2.5 keV), a grazing incidence optic has the greater efficiency; at higher energies (> ~2.5 keV), a polycapillary optic has greater efficiency (Figure 10). This choice results in two WDS spectrometer designs: one for high energy spectroscopy and one for low energy spectroscopy. (See the EDAX LEXS and TEXS product bulletins and the Bruker XSense flyer).

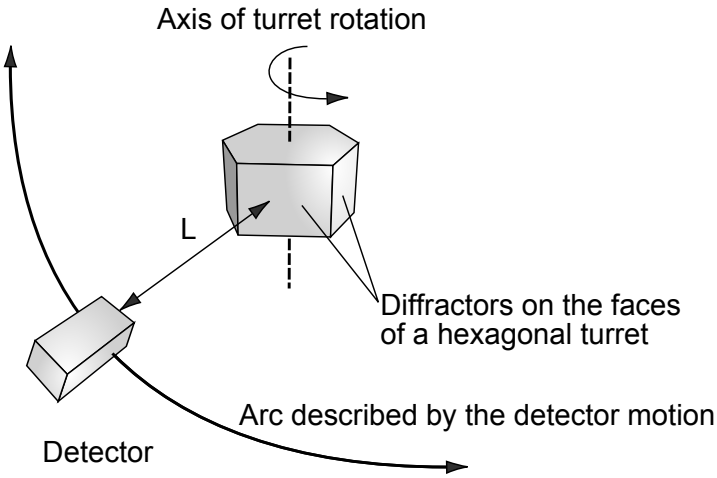

Figure 8: Schematic representation of a parallel beam spectrometer, showing a fixed L length movement of the detector, and diffractor turret.

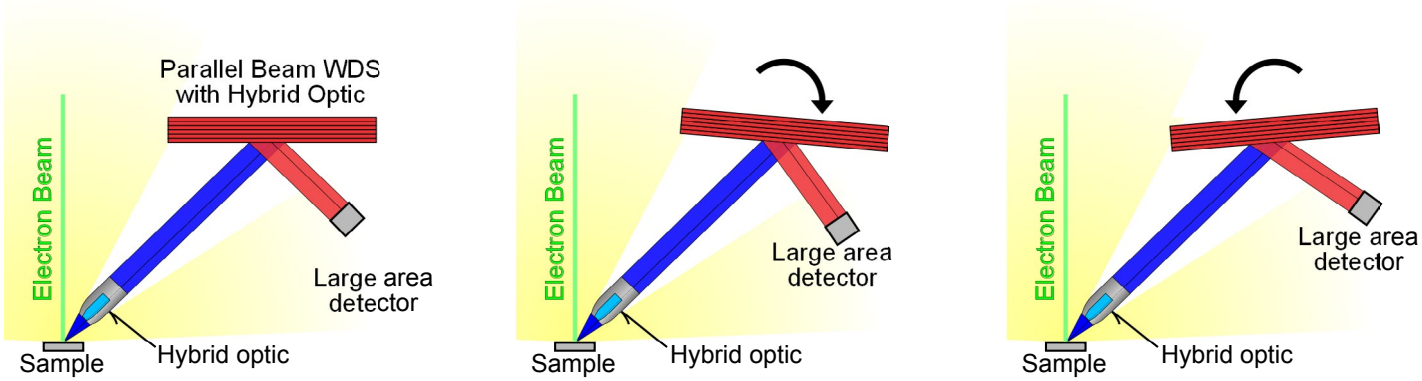

Figure 9: The yellow area represents all X-rays emitted from the sample by the interaction of the electron beam with the sample. The blue area represents the subset of X-rays that will collide with the diffractor. The red area represents the X-rays that are reflected by the diffractor to the detector. This diagram of a parallel beam WDS includes a hybrid optic consisting of both polycapillary and grazing incidence optics that transforms the divergent X-rays into a parallel beam, which reflect off the detector and are counted by the detector. However, this diagram would also be accurate for grazing incidence and polycapillary optics.

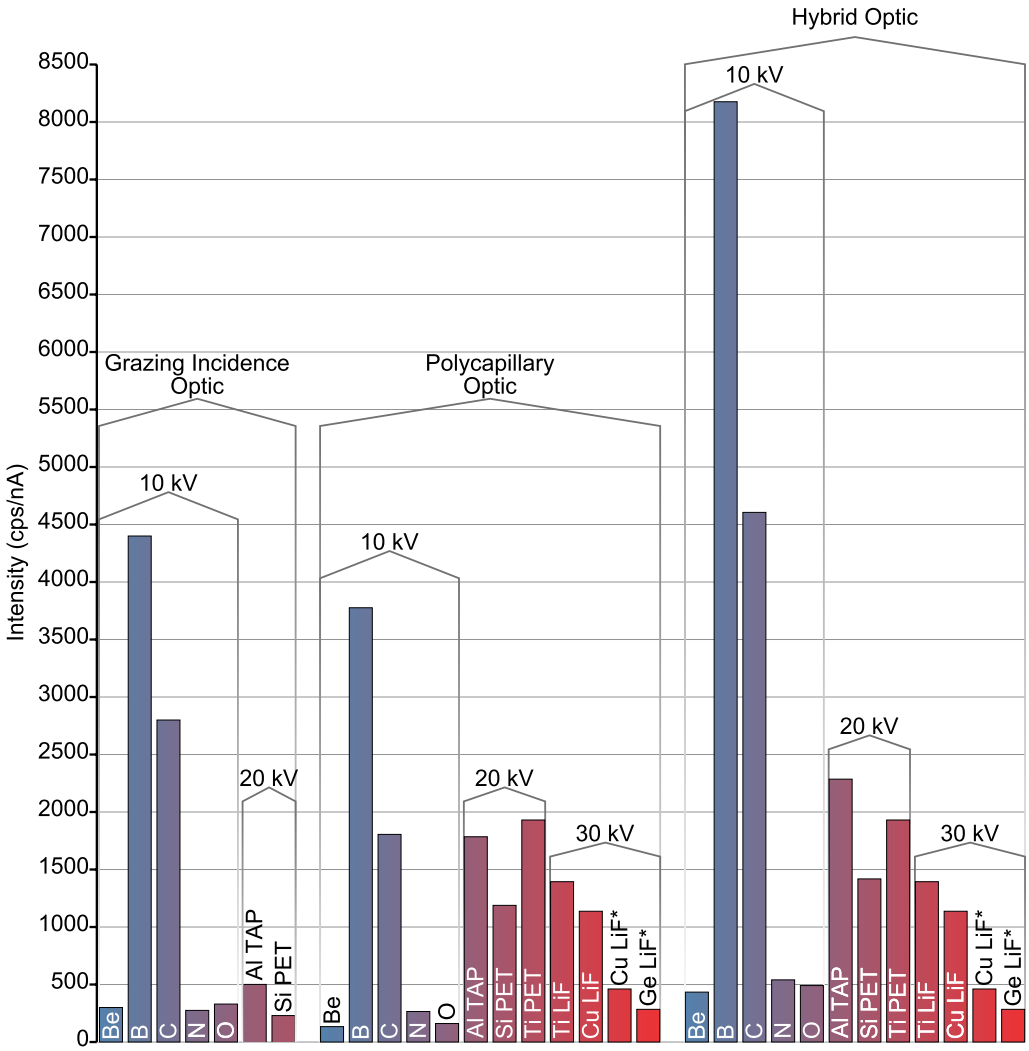

Figure 10: Expected intensities obtainable using parallel beam WDS spectrometers with (from left to right) a grazing incidence optic, a polycapillary optic, and a hybrid optic. Be, B, C, N, and O intensities are as would be obtained using layered diffractors with a 10 kV accelerating voltage. Al intensities are as would be obtained using a TAP crystal with a 20 kV accelerating voltage. Using a PET crystal, Si and Ti intensities are as would be obtained with a 20 kV accelerating voltage. Ti, Fe, Cu, and Ge are as would be obtained using LiF crystals with a 30 kV accelerating voltage. "LiF" refers to a LiF 200 crystal, and "LiF*" refers to a LiF 220 crystal. The difference between the two LiF crystals is that the LiF 220 has a smaller 2d spacing allowing it to be used for the analysis of higher energy X-rays compared to the more common LiF 200.

In parallel beam WDS systems, the sample and X-ray optic must be aligned properly with the sample at the proper working distance so that the parallel X-rays are incident on the diffractor. Deviations from the proper working distance can result in significant decreases in the detected X-ray intensity. This effect is greater for higher energy X-rays (e.g., Figure 11). In order to compensate for small deviations in sample position from the proper working distance, parallel beam WDS systems typically include routines that maximize the count rate of X-rays by either automatically adjusting the sample along the Z axis or by automatically adjusting the angle of the optic vertically and horizontally.

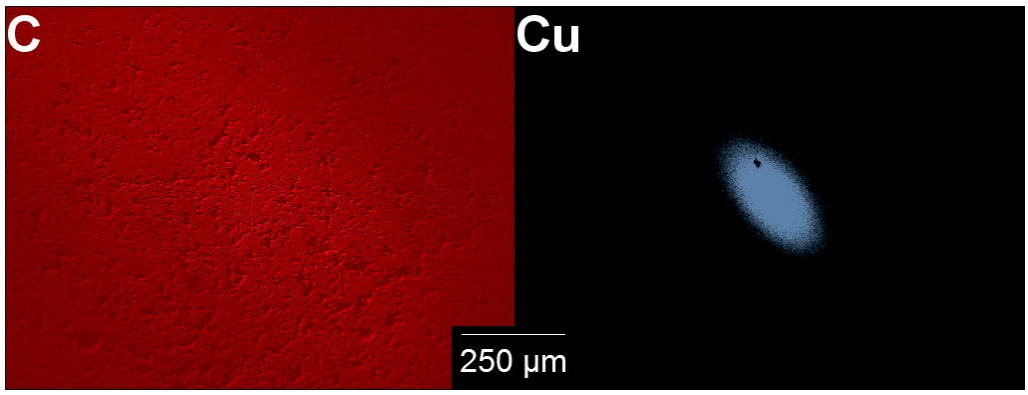

Figure 11: Low magnification parallel beam WDS maps for C Kα (0.282 keV) and Cu Kα (8.047 keV) of carbon and copper standards. The maps are generated by rastering the electron beam over the mapped area in contrast to moving the stage and sample underneath a fixed electron beam. Even if the sample is physically at the proper working distance from the pole piece of the SEM, the X-ray geometry is only appropriate at the point immediately below the pole piece. X-rays generated some distance away from this point are effectively not at the correct working distance. Therefore, the detected X-ray intensity decreases as a function of distance from the point on the sample immediately below the pole piece.

Parallel Beam WDS with a Hybrid Optic

The opportunity cost associated with choosing between high or low energy spectroscopy is eliminated by implementing a hybrid optic that incorporates both a grazing incidence and a polycapillary optic (Figure 7). The result is intense X-ray detection between 65 eV and 17.9 keV.

Application 1: Tricky Overlaps (i.e., Identification of Elements Unresolved by EDS)

Introduction

The energy resolution of EDS spectrometers is continually improving, but it cannot match the superior energy resolution of WDS. Peak deconvolution algorithms have been developed, which allow for the quantitative analysis of phases that yield EDS spectra with unresolved or partially unresolved EDS peaks. However, WDS is required to definitively determine the presence or absence of an element with characteristic X-ray lines that interfere with those another element, especially if one of the interfering elements is present at a trace concentration. This section gives three examples of common EDS peak overlaps and how WDS provides clarity.

The P-Y-Zr-Nb Interference

There are a few accessory minerals, which may occur in igneous or metamorphic rocks, that contain some combination of P, Y, Zr, and Nb (e.g., zirconolite, $(Ca,Fe,Y,REE)Zr(Ti,Nb)_2O_7$; xenotime, $(Y,HREE)PO_4$; yttrobetafite, $(Ca,Fe,Y,REE)_2(Ti,Nb)_2O_7$). These minerals are of interest as candidates for geochronology by electron-probe microanalysis (e.g., xenotime; Hetherington et al., 2008[8]) because they may contain wt%-level concentrations of Th, U, and, if old enough, radiogenic Pb. The commonly analyzed characteristic X-rays for these elements are P $K\alpha_{1,2}$ (2.015 keV), Y $L\alpha_1$ (1.922 keV), Zr $L\alpha_1$ (2.042 keV), and Nb $L\alpha_1$ (2.166 keV). Because these X-rays are, at best, 0.244 eV apart, they are not well-resolved in EDS (e.g., Y $L\alpha_1$ and Zr $L\alpha_1$; Figure 12).

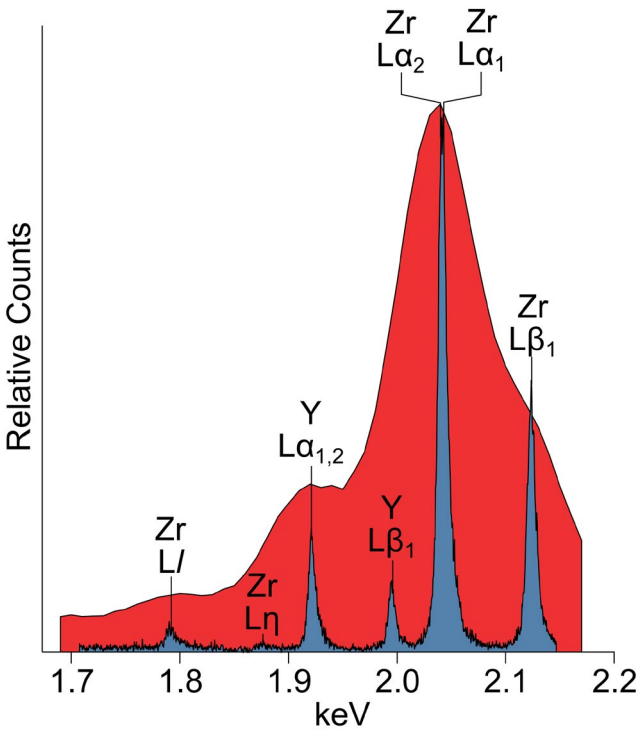

Figure 12: Red: Zr L-line portion of an ED spectrum of zirconia (ideally, ZrO_2) containing Y acquired using 15 kV. Blue: WDS energy scan of the same spectral region.

A xenotime grain occurring in a rock sample was analyzed using a parallel beam WDS with a hybrid optic. A WDS energy scan was done from 1693.5 to 2128.5 eV using a PET crystal as the diffractor (Figure 13).

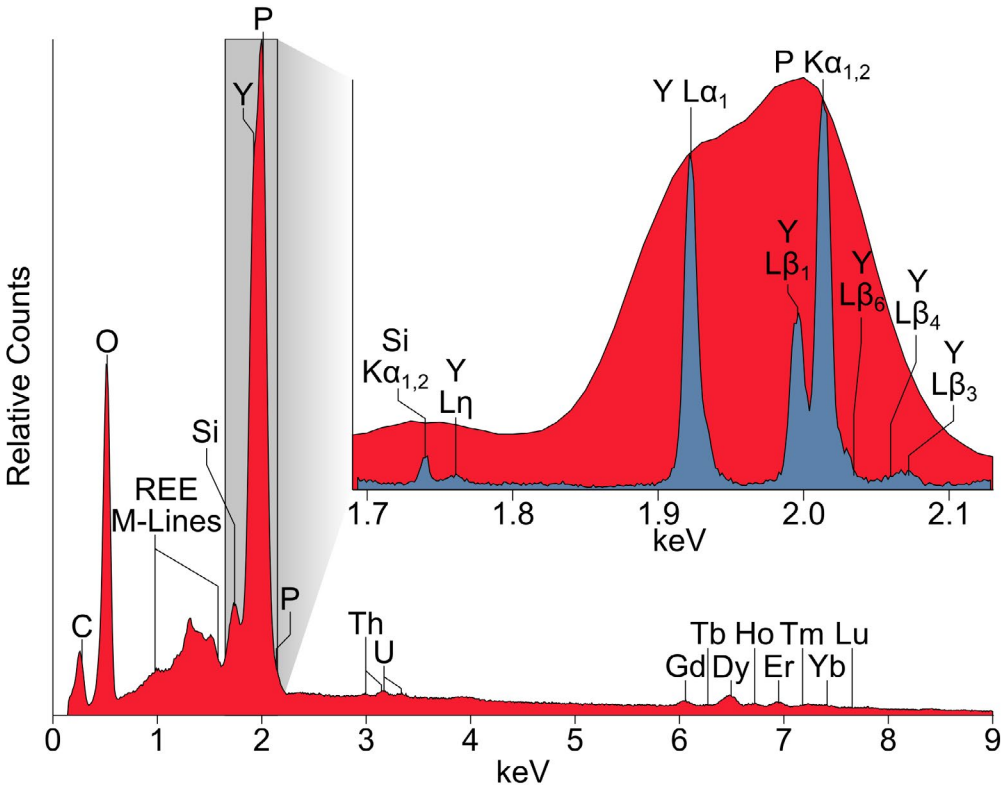

Figure 13: Main: ED spectrum of xenotime ([Y,REE] PO_4; REE = rare earth elements) acquired using 15 kV. Peaks, resolved and unresolved, are labeled. Inset: WDS energy scan (blue) and ED spectrum (red) of the same spectral region represented by the gray rectangle in the main image. Although partially resolved, P $K\alpha_{1,2}$ is not completely resolved from Y $L\beta_1$ and Y $L\beta_6$ and should not be used for WDS quantitative analysis.

Inspection of the EDS spectrum of xenotime (Figure 13) reveals a strong peak in the P $K\alpha_{1,2}$, Y $L\alpha_1$, Zr $L\alpha_1$, and Nb $L\alpha_1$ portion of the energy spectrum; however, it is difficult to definitely determine which of these elements are responsible for the peak. The WDS energy scan (Figure 13) readily resolves Y $L\alpha_1$ from P $K\alpha_{1,2}$ and partially resolves Y $L\beta_1$ from P $K\alpha_{1,2}$. Zr $L\alpha_1$ and Nb $L\alpha_1$ are not present in the WDS spectrum.

The Ti-V Interference (also known as a Z+1 interference)

So-called "Z+1 interferences" have always presented a challenge for EDS and WDS quantitative analysis. "Z+1 interference" refers to the interference of a Kβ X-ray line of an element of a given atomic number (Z) on the Kα line of the element with the atomic number of Z+1. Perhaps the most notorious Z+1 interference is that of Ti $K\beta_{1,3}$ on V $K\alpha_{1,2}$, which makes the identification of a small concentration of V in the presence of Ti difficult. There is both mineralogic and metallurgic interest in the identification of V in the presence of Ti. Given the similarities in ionic size and charge of Ti and V, a small concentration of V commonly occurs in Ti-rich minerals (e.g., ilmenite, $FeTiO_3$; rutile, TiO_2). Additionally, Ti and V are commonly alloyed with one another (e.g., Ti-6Al-4V).

A sample of Ti-6Al-4V alloy was analyzed using a parallel beam WDS with a hybrid optic. Two WDS energy scans were done on V-rich and V-poor phases in the alloy from 4850 to 5050 eV using a LiF crystal as the diffractor (Figure 14).

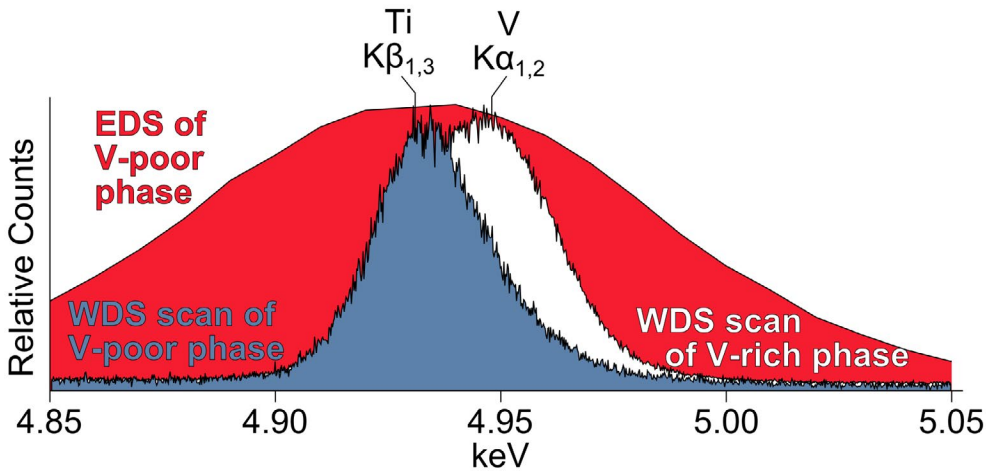

Figure 14: The Ti Kβ portion of the ED spectrum of Ti-6Al-4Valloy acquired using 15 kV (red). WDS energy scans from the V-poor phase (blue) and V-rich phase (white) of the same spectral region. The unresolved peak position shifts based on the relative concentrations of Ti and V.

The Ti $K\beta_{1,3}$ and V $K\alpha_{1,2}$ peaks are only separated by 17 eV, and WDS cannot fully resolve these peaks from one another. However, the relative concentration of Ti and V in the sample affects the position of the unresolved Ti $K\beta_{1,3}$ and V $K\alpha_{1,2}$ peak (Figure 14). In the energy scan of the V-rich phase, the unresolved peak is shifted toward the V $K\alpha_{1,2}$ position. In the energy scan of the V-poor phase, the unresolved peak is shifted toward the Ti $K\beta_{1,3}$ position.

The S-Mo-Pb Interference

The interferences of the S K-lines, the Mo L-Lines, and the Pb M-lines are notoriously difficult to deal with in EDS. Both Mo and Pb readily form sulfides (i.e., molybdenite, MoS_2; galena, PbS). Moreover, given the health ramifications associated with Pb, there is strong motivation to be sure that a material that contains S and/or Mo is free of Pb.

A galena grain in a rock sample and a MoS_2 sample were analyzed using a parallel beam WDS with a hybrid optic. A WDS energy scan was done from 2108.0 to 2749.5 eV using a PET crystal as the diffractor (Figure 13).

From the inspection of the EDS spectrum of galena (Figure 15), it is difficult to determine which elements are present. The WDS energy scan (Figure 15) readily resolves S $K\alpha_{1,2}$ from Pb $M\alpha_{1,2}$. Additionally, a small Mo $L\beta_1$ peak is present. Because of the low Mo concentration in the galena grain, Mo $L\alpha_{1,2}$ is unresolved from S $K\alpha_{1,2}$. Without WDS, the presence of Mo in the sample would not have been identified.

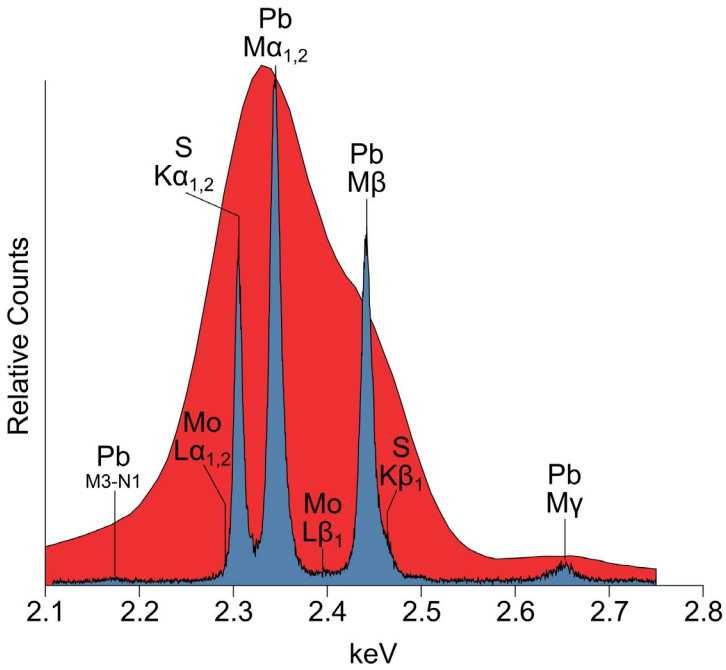

Figure 15: Red: S-Mo-Pb portion of an ED spectrum of galena (ideally, PbS) using 15 kV. Blue: WDS energy scan of the same spectral region. The presence of Mo $L\beta_1$ indicates a small concentration of Mo in the galena. The Mo $L\alpha_{1,2}$ line, which should also be present if Mo $L\beta_1$ is present, is unresolved from S $K\alpha_{1,2}$.

Examination of the MoS_2 sample by WDS reveals that Mo $L\alpha_{1,2}$ and S $K\alpha_{1,2}$ are represented as shoulders on an unresolved peak at ~2.3 keV (Figure 16). Additionally, S $K\beta_1$ is unresolved from Mo $L\beta_{4,6}$ and Mo $L\beta_3$.

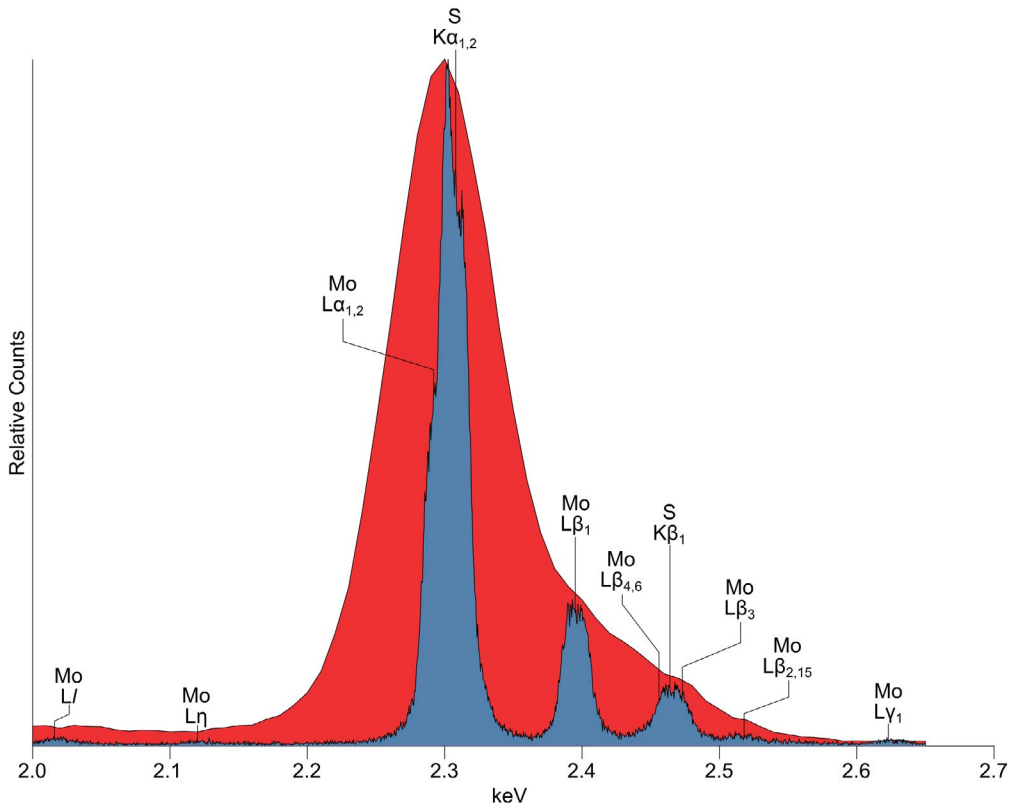

Figure 16: Red: S-Mo-Pb portion of an ED spectrum of MoS_2 using 20 kV. Blue: WDS energy scan of the same spectral region. Mo $L\alpha_{1,2}$ and S $K\alpha_{1,2}$ are represented as shoulders on an unresolved peak at ~2.3 keV. S $K\beta_1$ is unresolved from Mo $L\beta_{4,6}$ and Mo $L\beta_3$. Several low-intensity Mo L-lines are present in the WDS spectrum.

The Ti-Ba Interference

Ba $L\alpha_1$ and Ti $K\alpha_{1,2}$ are unresolved in EDS. Ba and Ti are elements that are common components in metals (Ti), ceramics, and minerals. Therefore, it is useful to know whether one of both of these elements are present in a sample.

A sample of synthetic $BaTiO_3$, which naturally occurs as barioperovskite (Ma and Rossman, 2008[9]), was analyzed using a parallel beam WDS with a hybrid optic. A WDS energy scan was done from 4300 to 5000 eV using a LiF crystal as the diffractor (Figure 17).

In the WDS energy scan (Figure 17), Ba $L\alpha_1$ and Ti $K\alpha_{1,2}$ are almost completely resolved from one another, but they are not resolved in EDS.

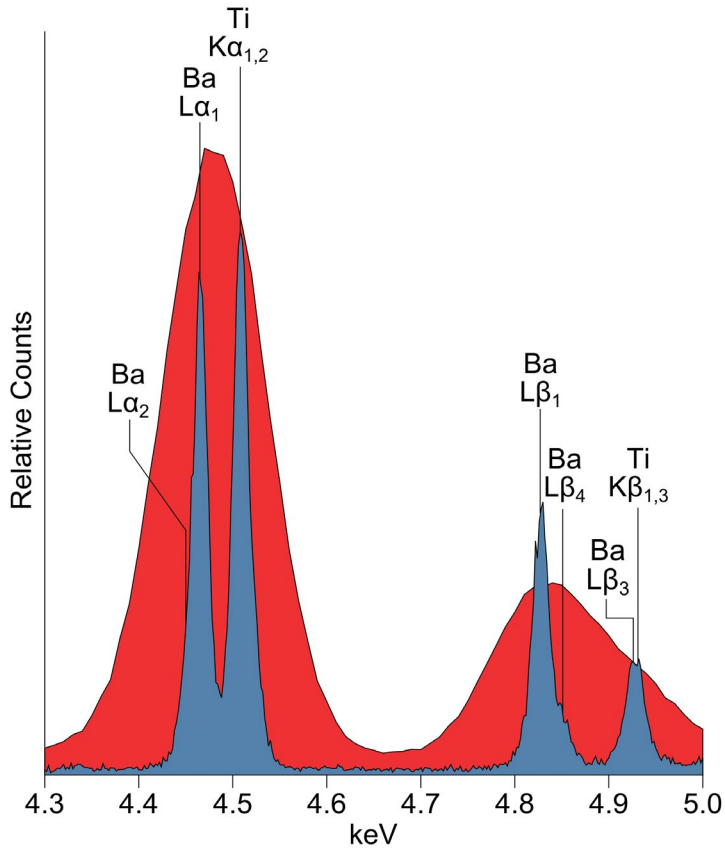

Figure 17: Red: portion of an ED spectrum of synthetic $BaTiO_3$ using 20 kV. Blue: WDS energy scan of the same spectral region. Ba $L\alpha_1$ and Ti $K\alpha_{1,2}$ are unresolved in EDS but partially resolved in WDS.

Application 2: Quantitative Analysis

Introduction

As with all quantitative analysis, the analysis of Freibergite requires a systematic approach. Freibergite ($[Cu,Zn,Ag]_{12}[Sb,As]_4S_{13}$), a mineral of interest because it is mined as an Ag ore, contains six elements, three (As, Ag, and Sb) of which are most practically measured using their L-lines at typical accelerating voltages. The L-line family consists of several peaks that may or may not all be resolvable using WDS and may or may not all be above the background depending of the concentration of the element generating the L-lines.

WDS quantitative analysis requires the measurement of X-rays on- and off-peak in order to determine peak intensity, involving no peak deconvolution methodology. Therefore, in order for WDS quantitative results to be accurate, it is essential that the peak to be measured is free of interferences and that the off-peak measurement positions are truly representative of the background. Regarding on-peak interferences, in some cases, interferences are not resolvable by a WDS energy scan (e.g., Ti $K\beta_{1,3}$ on V $K\alpha_{1,2}$; Figure 14). In other cases, interferences may be partially resolvable by a WDS energy scan (e.g., Y $L\beta_1$ on P $K\alpha_{1,2}$; Figure 13); however, if the high or low energy peak tails of the interfering X-ray line are not at background levels at the on-peak position, the quantitative results will be incorrect. In Figure 13, P $K\alpha_{1,2}$ should not be measured for quantitative analysis because it is unlikely that the high energy peak tail of Y $L\beta_1$ is at the background. The effect of measuring on a peak bearing an unresolved or partially resolved interference is the over-estimation of the measured element.

In WDS, X-ray line intensities are determined by calculating the peak height above the background. If the background measurements are inadvertently made on a peak instead of the background, the concentration of the measured element will be under-estimated. The determination of off-peak measurement positions can be more challenging when measuring L- or M-lines because of the presence of several satellite peaks in those X-ray line families (e.g., Figure 18). In order to ensure that the on-peak position is free of interferences and that the off-peak positions do not fall on a neighboring peak, a WDS energy scan should be acquired of the spectral region of interest.

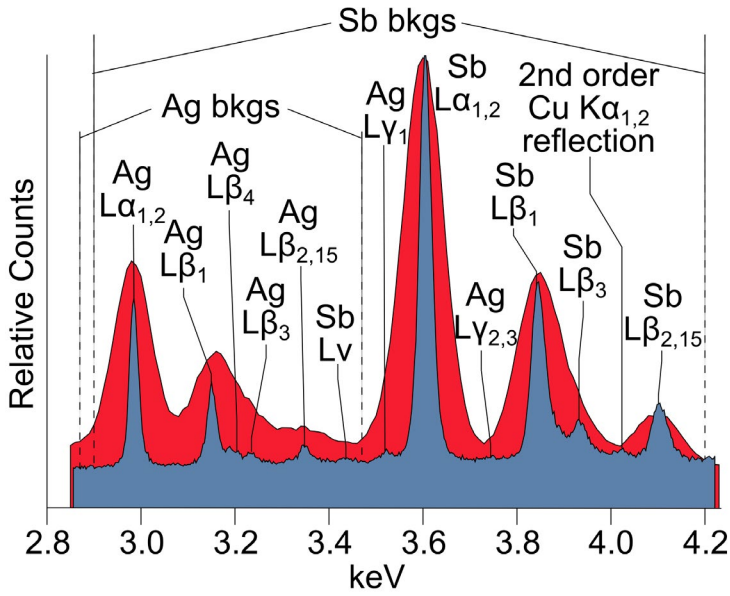

Figure 18: WDS energy scan (blue) and ED spectrum (red) of the same spectral region acquired from freibergite at 15 kV. The presence of the many satellite peaks of the Ag and Sb L-line families, as well as a 2nd order reflection of Cu Kα, illustrates the importance of choosing off-peak measurement positions based on the meticulous inspection of WDS energy scans.

Methods

Quantitative WDS analysis of freibergite was done using a parallel beam WDS with a hybrid optic on an FESEM. The sample was polished and carbon coated. Analytical conditions were an accelerating voltage of 15 kV and a beam current of 27 nA. Standardization was done using natural and synthetic mineral standards.

Results

The results of the WDS quantitative analysis of freibergite are tabulated in Table 1. The composition corresponds to a mineral formula of $(Cu,Ag)_{10.2}(Zn)_{1.9}(Sb,As)_{4.2}S_{13}$ and is consistent with other reported analyses of the mineral freibergite done using electron-probe microanalysis (Anthony et al., 2014[10]).

Table 1: Composition of freibergite determined by WDS quantitative analysis using a parallel beam WDS with a hybrid optic. Reported values are averages from 13 analyses.

Element	Average (wt%)	σ
N	13	–
S	23.7	0.45
Cu	30.3	1.44
Zn	7.15	0.54
As	2.16	0.82
Ag	11.4	1.86
Sb	25.4	1.17
Total	**100.2**	

Application 3: WDS Mapplications

Introduction

Peak overlaps such as those discussed in Application 1 can also confound X-ray maps, typically resulting in false positives or the mapping of incorrect elements. Mapping with WDS eliminates the effect of many of these overlaps. Additionally, the low background of WDS allows for trace elements to be mapped that cannot be mapped with EDS because of their low concentration.

Methods

WDS maps of a Sn electrode with a layer of Ni insulating Cu from Sn were generated by rastering the beam over the sample. Because the width of the Ni layer was thin (~1 µm), a low accelerating voltage was used to minimize the electron probe interaction volume. X-rays were counted using a parallel beam WDS with a hybrid optic and using a TAP crystal as the diffractor. A WDS map of a steel containing B was generated concurrently with an EDS image cube by rastering the beam over the sample. X-rays were counted using a parallel beam WDS with a hybrid optic and using a layered diffractor and an SDD (for EDS).

Results

Because the L-lines of Ni and Cu strongly overlap, the Ni and Cu EDS maps are similar (Figure 19). In the Ni EDS map, the Cu and the Ni layers are nearly indistinguishable. However, in the WDS maps (Figure 19), the Ni layer is clearly distinguished from the Cu layer.

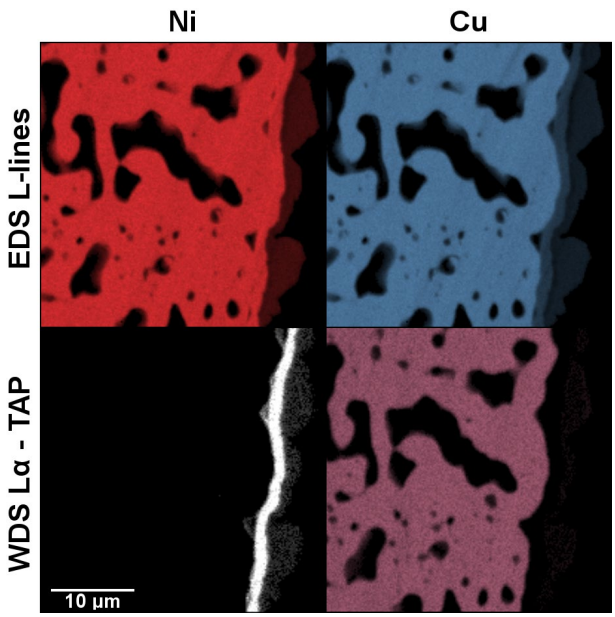

Figure 19: Ni (upper left) and Cu (upper right) EDS maps generated using the L-lines. The Ni EDS maps contains a strong contribution from Cu. The Cu EDS map contains a lesser contribution from Ni. The Ni Lα (lower left) and Cu Lα (lower right) WDS maps do not contain contributions from other elements.

In EDS, B is poorly mapped by raw counts (Figure 20, top). Mapping the B net counts from EDS reveals a single phase that contains B, but the counts are low (Figure 20, middle). However, WDS yields a rich B map, revealing three Fe-Cr phases with different B concentrations (Figure 20, bottom).

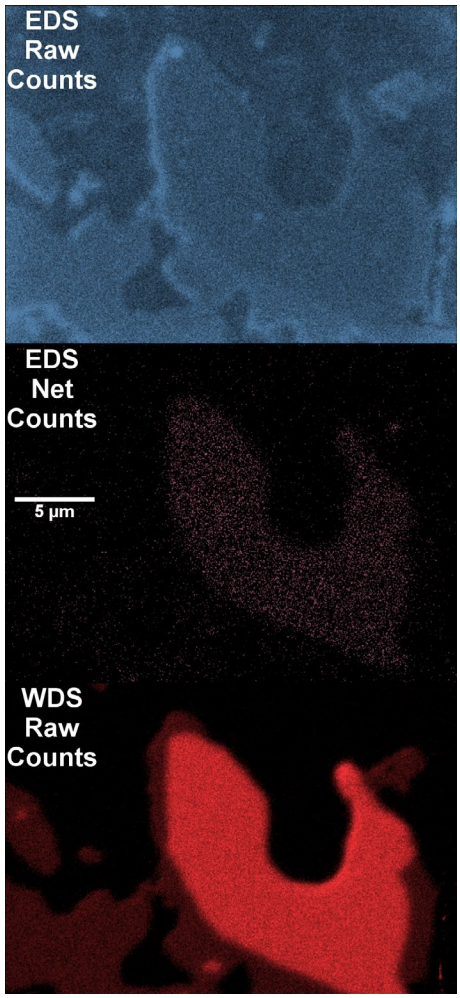

Figure 20: Boron X-ray maps of concurrently acquired EDS raw counts, EDS net counts, and WDS raw counts in a sample of steel containing boron.

Conclusions

Compared with EDS, WDS offers significant resolution improvements with peak overlaps virtually eliminated. An order of magnitude improvement in peak-to-background sensitivity enhances trace element detection. Parallel beam WDS gives a great improvement in intensity in the low energy spectral region, in which most overlaps occur, in comparison to conventional WDS.

Parallel beam WDS with a hybrid optic, in comparison to conventional WDS, gives a great improvement in resolution in the low energy spectral region where most overlaps occur.

The better peak-to-background and elimination of overlaps yield more accurate quantitative analysis for those elements in low concentration or involved in the overlap. Because the WD spectrometer can be positioned at the center of the peak, where peak-to-background is maximized, WDS provides superior X-ray maps, especially for low concentration

Because of the serial nature of spectrum acquisition, qualitative analysis is slow compared to EDS. However, because WDS is often operated by driving the crystal directly to the peak, counting time is devoted only to the points of real interest. For minor elements, WDS then becomes fast relative to EDS, in which most counted X-rays will originate from the major elements. Parallel beam WDS empowers the SEM user to do quantitative analysis with the same rigor and accuracy achieved by electron-probe microanalysis.

References

1. Castaing, R. (1951) Ph.D. Thesis, University of Paris.
2. JEOL L-Value table www.jeolusa.com/DesktopModules/Bring2mind/DMX/Download.aspx?EntryId=620&PortalId=2&DownloadMethod=attachment
3. CAMECA SXFiveFE brochure www.cameca.com/download/CAMECA%20SXFiveFE%202%20page%20flyer.pdf
4. Oxford Instruments Wave brochure http://www.oxford-instruments.com/OxfordInstruments/media/nanoanalysis/brochures%20and%20thumbs/WDS_brochure.pdf
5. Thermo Electron Corporation, (2001) WDS Theory of Operations, IbeX http://www.thermo.com/eThermo/CMA/PDFs/Articles/articlesFile_10834.pdf
6. EDAX LEXS product bulletin http://www.edax.com/download/LEXS_PB.pdf
7. Bruker XSense flyer. http://www.bruker.com/fileadmin/user_upload/8-PDF-Docs/X-rayDiffraction_ElementalAnalysis/Microanalysis_EBSD/Flyers/Fly_xsense_en_rev1_0_lowres.pdf
8. Hetherington, C.J., Jercinovic, M.J., Williams, M.L., and Mahan, K. (2008) Understanding geologic processes with xenotime: Composition, chronology, and a protocol for electron probe microanalysis. Chemical Geology, 254, 133–147.
9. Ma, C., and Rossman, G.R. (2008) Barioperovskite, $BaTiO_3$, a new mineral from the Benitoite Mine, California. American Mineralogist, 93, 154–157.
10. Anthony, J.W., Bideaux, R.A., Bladh, K.W., Nichols, M.C., Eds., Handbook of Mineralogy, Mineralogical Society of America, Chantilly, VA 20151-1110, USA. http://www.handbookofmineralogy.org/

Africa +43 1 333 50 34 0
Australia +61 3 9757 4300
Austria +43 810 282 206
Belgium +32 53 73 42 41
Canada +1 800 530 8447
China +86 21 6865 4588
Denmark +45 70 23 62 60
Europe-Other +43 1 333 50 34 0
Finland/Norway/Sweden +46 8 556 468 00
France +33 1 60 92 48 00
Germany +49 6103 408 1014
India +91 22 6742 9494
Italy +39 02 950 591
Japan +81 45 453 9100
Latin America +1 561 688 8700
Middle East +43 1 333 50 34 0
Netherlands +31 76 579 55 55
New Zealand +64 9 980 6700
Russia/CIS +43 1 333 50 34 0
Spain +34 914 845 965
Switzerland +41 61 716 77 00
UK +44 1442 233555
USA +1 800 532 4752

WP52608_E 10/14M

Thermo SCIENTIFIC
A Thermo Fisher Scientific Brand